

Quantum walk versus stone in pond: Distinguishing ground states of quantum magnets by spacetime dynamics

Piotr Wrzosek,¹ Krzysztof Wohlfeld,^{1,*} Tomasz Sowiński,^{2,†} and Michael A. Sentef^{3,‡}

¹*Faculty of Physics, University of Warsaw, Pasteura 5, PL-02093 Warsaw, Poland*

²*Institute of Physics, Polish Academy of Sciences, Aleja Lotników 32/46, PL-02668 Warsaw, Poland*

³*Max Planck Institute for the Structure and Dynamics of Matter, Luruper Chaussee 149, D-22761 Hamburg, Germany*

(Dated: August 31, 2022)

We investigate the wavepacket spreading after a single spin flip in prototypical two-dimensional ferromagnetic and antiferromagnetic quantum spin systems. We find characteristic spatial magnon density profiles: While the ferromagnet shows a square-shaped pattern reflecting the underlying lattice structure, as exhibited by quantum walkers, the antiferromagnet shows a circular-shaped pattern which hides the lattice structure and instead resembles the wave pattern of a stone thrown into a pond. We trace these fundamentally different behaviors back to the distinctly different magnon energy-momentum dispersion relations and also provide a real-space interpretation. Our findings point to new opportunities for real-time, real-space imaging of quantum magnets both in materials science and in quantum simulators.

Two-dimensional quantum magnets are quintessential quantum many-body systems that come in two main realizations: antiferromagnets (AF) or ferromagnets (FM). AF are prototypical condensates (BCS superconductors, superfluids, crystals), in which classical order is dressed by its associated quantum fluctuations [1]. Whereas the latter do not destroy the order at $T = 0$ – as would happen for AF chains, in agreement with the Coleman theorem – the quantum reduction of the order parameter is of the order of 40%. Such strong quantum effects are intrinsically related to the onset of the low-lying excitations above the respective ground state (Goldstone modes), which are coined magnons and have linear-in-momentum ($|\mathbf{k}|$) quasi-particle dispersion. By contrast, FM can be regarded as more unique because their fully polarized ground state does not contain any quantum fluctuations, and the low-lying excitations disperse as \mathbf{k}^2 . Hence the FM ground state can be viewed a natural realization of a true vacuum, and the associated magnon excitations as particles.

In traditional condensed matter physics the questions of magnetic ground states and their associated low-lying excitations on the atomic length scale are investigated experimentally with scattering techniques (neutrons, X-rays), which yield information in reciprocal space (momentum \mathbf{k} , frequency ω). On the other hand, tremendous progress in controlling ultracold gases in optical lattices has provided a complementary real-space and real-time (\mathbf{r}, t) perspective on archetypal spin Hamiltonians [2, 3]. Due to the tunability of these systems, it is now possible to perform quantum simulations of systems described by celebrated Hamiltonians previously considered as minimal toy models, such as the fermionic [4, 5] and bosonic [6] Hubbard model, the Ising model [7], and the Heisenberg model [8]. The spacetime-resolved microscopic imaging of such quantum simulators is possible thanks to the single-site fluorescence imaging technique invented almost decade ago [9–11], and further developed

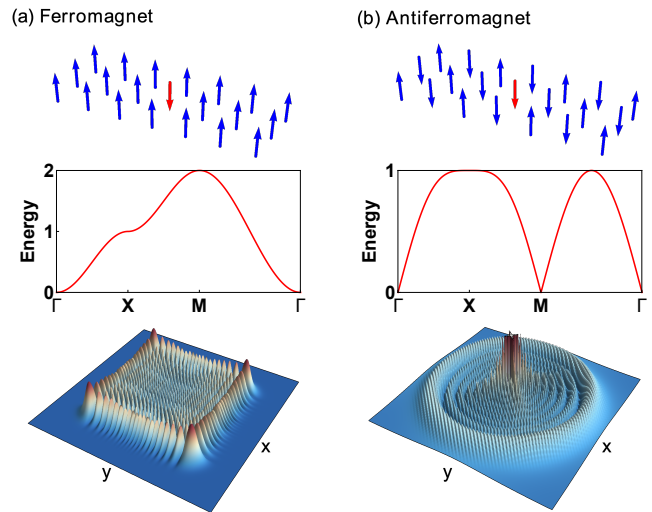


Figure 1. **Single-magnon excitation properties in two-dimensional quantum magnets.** (a) Ferromagnet, (b) antiferromagnet. Top row: Cartoon of the ground state with a single spin flip (red). Middle row: Dispersion relation of single-magnon excitations, with \mathbf{k}^2 (FM) and $|\mathbf{k}|$ (AF) low-energy behavior around Γ , respectively. Bottom row: Snapshot of spatial density profile for $t \sim 30$ fs after spin-flip excitation. Spin exchange is taken to be a representative value of $J = 100$ meV.

recently [12–17]. In particular, this technique was successfully used for the quantum simulation and the spacetime probing of AF order in a two-dimensional lattice [18].

In this Letter, we take a fresh look at the old problem of magnetic ground states and their low-lying excitations focussing on generic 2D square-lattice quantum magnets. We examine the spacetime dynamics of a single initially localized excitation on top of the respective magnetic ground state. We find simple yet remarkable and robust distinguishing fingerprints between the FM

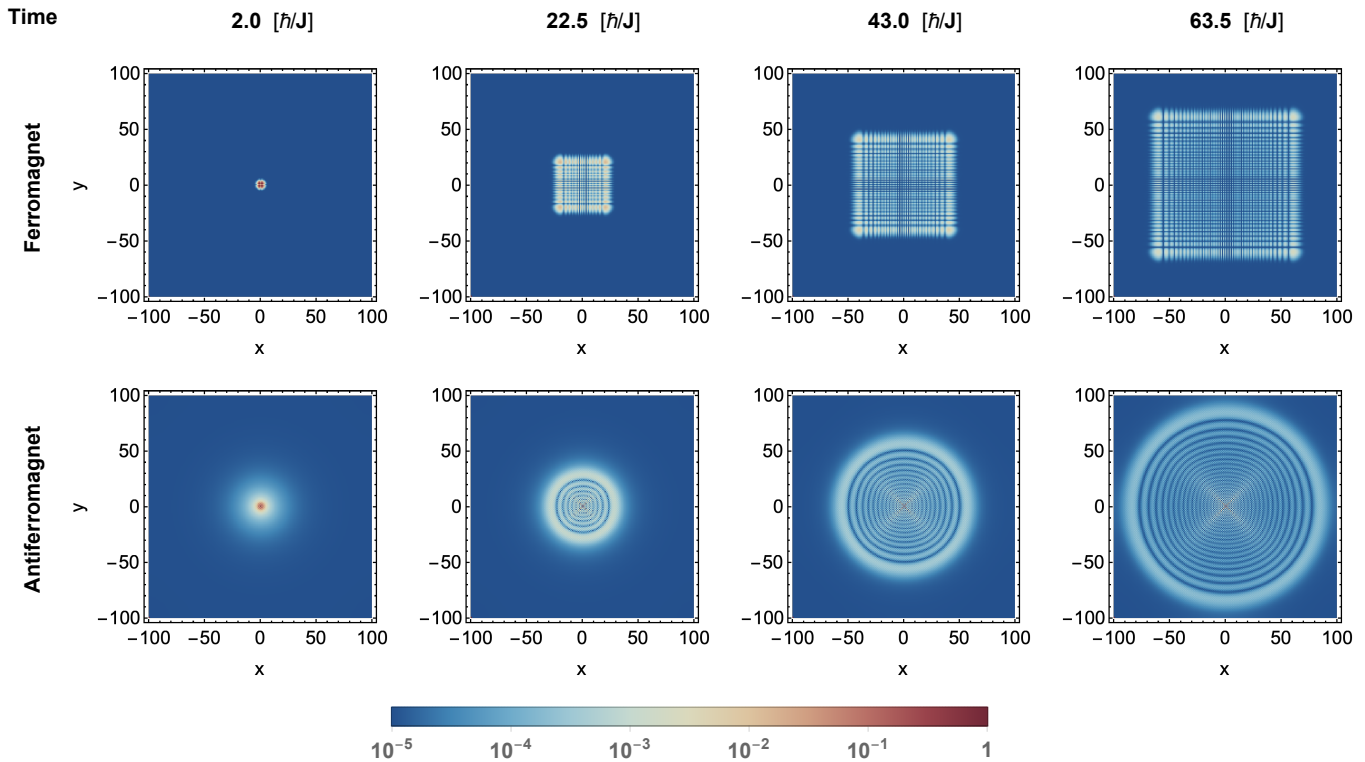


Figure 2. **Snapshots of spatiotemporal evolution of the density profiles.** Panels show the respective real-space density profiles after spin flip at position $(x = 0, y = 0)$ and time $t = 0$ for the ferromagnet (top row) and antiferromagnet (bottom row), respectively. Columns correspond to different waiting times after excitation as indicated.

and AF cases. In the FM case the problem is readily mapped onto the problem of a single quantum particle in the vacuum. Thus it is classified as the well-known quantum walk in continuous time on a discrete spatial lattice, which recently is under extensive theoretical and experimental exploration [19–29]. As expected from intuition based on this analogy, a square pattern emerges in the spatial density profile after excitation, reflecting the underlying crystal symmetry (Fig. 1(a)). By striking contrast, the dynamics above the AF ground state is instead reminiscent of a stone thrown into a pond, with isotropic circular patterns largely ignorant of the crystal symmetry (Fig. 1(b)). We trace this quantum-walk versus stone-in-pond behavior back to the fundamental difference in quantum ground states and their associated low-energy excitations.

Consider the 2D spin $S = \frac{1}{2}$ Heisenberg model

$$\hat{H} = J \sum_{\langle i,j \rangle} \hat{\mathbf{S}}_i \cdot \hat{\mathbf{S}}_j + h \sum_i \hat{S}_i^z, \quad (1)$$

on a 2D square lattice with nearest-neighbor spin exchange coupling $J > 0$ and external magnetic field h polarized along the z axis. In the following we discuss the two limits (i) $h = 4J$ (FM) and (ii) $h = 0$ (AF). The physics of this model in the canted AF regime $0 < h < 4J$ constitutes a crossover case whose qualitative

understanding can be easily obtained from the FM and AF cases.

In the following we will investigate the dynamics of a single spin-flip on top of the ground state of the Hamiltonian (1) by the Holstein-Primakoff linear spin-wave (LSW) theory (see, e.g., [30] or [31] for details), mapping spin operators on site j to canonical bosonic operators and truncating at the leading order in $\frac{1}{S}$ via $\hat{S}_j^z = \frac{1}{2} - \hat{a}_j^\dagger \hat{a}_j$, $\hat{S}_j^+ \approx \hat{a}_j$ and $\hat{S}_j^- \approx \hat{a}_j^\dagger$. After performing a Fourier transformation to momentum space and a Bogolyubov transformation (see supplementary material [32] for details) one arrives at the approximate LSW version of the Hamiltonian in terms of Bogolyubov magnons $\hat{\alpha}_{\mathbf{k}}^\dagger$,

$$\hat{H} = \sum_{\mathbf{k}} \omega_{\mathbf{k}} \hat{\alpha}_{\mathbf{k}}^\dagger \hat{\alpha}_{\mathbf{k}} + \frac{1}{2} \sum_{\mathbf{k}} (\omega_{\mathbf{k}} - (2J(1 + \gamma_{\mathbf{k}} \sin^2 \theta))), \quad (2a)$$

with magnon dispersion

$$\omega_{\mathbf{k}} = 2J \sqrt{(1 + \gamma_{\mathbf{k}})(1 - \gamma_{\mathbf{k}} \cos 2\theta)}, \quad (2b)$$

where $\gamma_{\mathbf{k}} = \frac{1}{2}(\cos k_x + \cos k_y)$ and $\sin \theta = \frac{h}{4J}$. We note that one can map case (i) to the usual Heisenberg FM with $J < 0$ by a (π, π) shift in momentum space, which leads to the FM magnon dispersion with minimum at Γ as shown in Fig. 1(a).

We start from the ground state of the LSW Hamiltonian (2a), which is given by the magnon vacuum $|\varnothing_\alpha\rangle$. We note that this is the exact ground state (fully polarized state) for the FM case, while it is the approximate ground state for the AF case as it neglects additional quantum fluctuations caused by magnon-magnon interactions. We define the following protocol for the dynamics. Starting from the ground state as the initial state, we apply at time $t = 0$ a single spin-flip operator locally on site at $\mathbf{r} = \mathbf{r}_0 = 0$, which amounts to creating a single boson. Then we compute the spatiotemporal excitation density profile, which in the language of the Holstein-Primakoff magnons can be written as

$$\rho(\mathbf{r}, t) = \langle \varnothing_\alpha | \hat{a}_{\mathbf{r}_0}(t) \hat{n}_{\mathbf{r}_i} \hat{a}_{\mathbf{r}_0}^\dagger(t) | \varnothing_\alpha \rangle, \quad (3)$$

where $\hat{a}_{\mathbf{r}}^\dagger(t) = e^{-i\frac{\hat{H}}{\hbar}t} \hat{a}_{\mathbf{r}}^\dagger \sqrt{1 - \hat{a}_{\mathbf{r}}^\dagger \hat{a}_{\mathbf{r}}}$. In this way we have access to the spacetime dynamics of the distribution of excitations in the lattice. A detailed explanation is provided in the supplementary material [32].

The main result, presented in Fig. 1, is the distinct density profile of spin excitations created in the FM and AF background. While the FM case resembles a quantum walker with a square pattern that reflects the underlying lattice structure, the AF case resembles a stone thrown into a pond with a circular pattern that is quasi-ignorant of the underlying microscopic lattice. In the momentum space picture, this can be understood by considering the respective magnon dispersion relations. For the FM (Fig. 1(a)) the dispersion is quadratic ($\propto \mathbf{k}^2$) near Γ , and its largest slope, and therefore the highest magnon velocity, stems from other parts of the Brillouin zone. Since the local spin flip is composed of all momenta in the Brillouin zone, its spread velocity is dominated by those fast components, which reflect the lattice structure. By striking contrast, for the AF case the dispersion is linear ($\propto |\mathbf{k}|$) near Γ , where it also has its largest slope. Therefore the spread of the spin-flip excitation is dominated by the momentum-space region near Γ , with its emergent isotropic symmetry at long wavelengths, ignorant of the underlying square lattice. On top of that, the quantum fluctuations encoded in the Bogolyubov transformation additionally put a stronger focus on the Γ point region for the AF case, since the coherence factors modulate the contributions from different momentum-space regions to the wave packet dynamics (for details see supplementary material [32]). As an important consequence of these arguments, the observed striking differences in the spacetime dynamics between FM and AF are expected to be largely insensitive to the details of the prepared initial state, as long as it is sufficiently localized, and also insensitive to the details of the Hamiltonian realizations.

We now elucidate the emergence in real time of the patterns discussed here. In Fig. 2 we show snapshots of the time evolution of the density profile for the FM (top row) and AF (bottom row) cases. Interestingly, in both cases

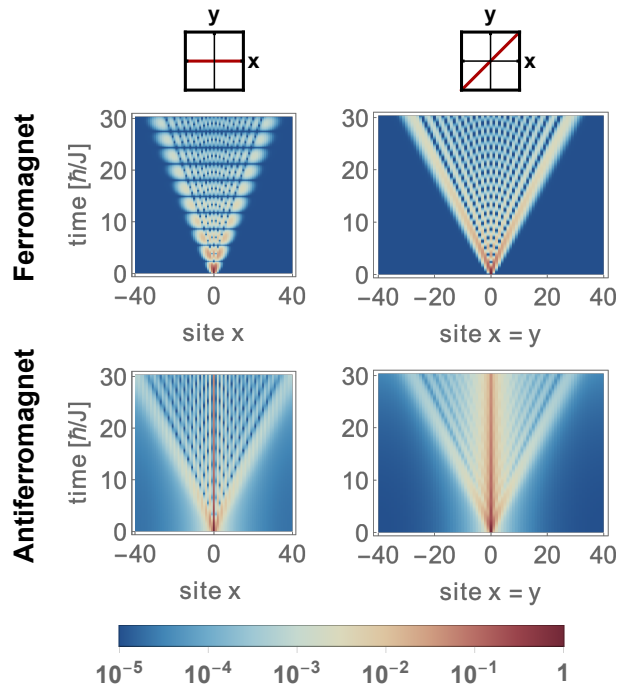


Figure 3. **Light-cone-like structures along selected real-space cuts.** Spatial cuts of density profiles along x (left panels) and along $x - y$ diagonal (right panels) for the FM (top) and AF (bottom) cases, respectively.

the characteristic density profiles emerge quickly between the earliest times ($2.0\hbar/J$) and the next snapshots shown here at $22.5\hbar/J$. At increasingly longer times, we find the development of self-similar patterns for both FM and AF cases, with a speed of expansion that remains constant over time. This observation is in line with the above momentum-space interpretation: the wave fronts of the density profiles evolve according to the fastest available velocities in the respective wave packets.

In order to highlight this constant-velocity spreading and to also investigate some more subtle differences between the FM and AF, we present in Fig. 3 the density profiles along selected real-space cuts in the 2D lattice as functions of time. In the FM case, for the spreading along the x direction, and by symmetry also along the y direction (not shown), one observes a well-known light-cone-like structure [33]. In the diagonal direction, one also observes a similar light cone but with a velocity that is larger by a factor of $\sqrt{2}$, again highlighting the momentum-space picture discussed above, and leading to the characteristic square-shaped density profile of the quantum walker. On top of these overall features, we also note that the highest density is found at the edge of the light cone for the FM case. This latter more detailed feature is in stark contrast to the AF case. In the AF, the highest density remains at the center of the excitation. Moreover, as already discussed, the stone-in-pond circular-shaped picture emerges because the light

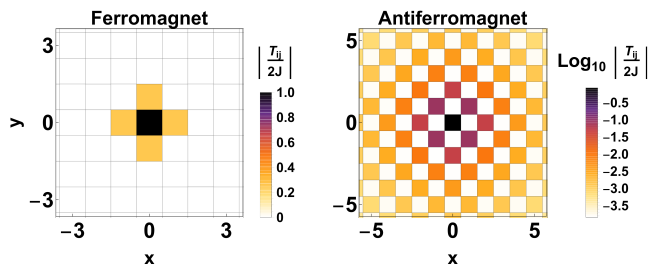


Figure 4. **Real-space effective hopping interpretation of quantum walk versus stone in pond.** The tunneling amplitudes $|T_{ij}/2J|$ shown on a square lattice for FM (left panel) and AF (right panel) groundstate, respectively.

cone spreads isotropically, i.e., equally fast both along the crystal axes and along the diagonal.

Let us briefly comment on why the spatial magnon density profiles resemble the observed light-cone-like structures. A priori this should not be expected, since the magnon propagation happens via the evolution operator $e^{-i\hat{H}t}$, and one could naively expect that the magnon wave function would have nonzero values on all lattice sites for all times $t > 0$. This paradox is resolved by observing that in fact the light cones are not sharply defined—a magnification of the magnon density profile shows that the probabilities of detecting a magnon excitation outside the cone is nonzero, even though it quickly decays (see Fig. S1 in the supplementary material [32]).

Finally, we will provide a comprehensive real-space understanding of the observed cone-like spreading and real-space structures. To this end we will split the problem into three steps.

(i) Explanation of a finite density of magnons along the abscissa axis already at time $t = 0$ in the AF case (bottom panel in Fig. 3 and Fig. S2 in the supplementary material [32]). This can be clarified by investigating consequences of a single spin flip (a magnon *before* Bogolyubov transformation) at the initial time. It is clear that the single Bogolyubov magnon at site \mathbf{r}_0 , which is a Fourier-transformed eigenstate of the system, is a superposition of spin flips whose real-space distribution decays with distance from site \mathbf{r}_0 (for more details see the supplementary material [32]). This originates in the fact that the Hamiltonian makes it energetically favorable to cluster the magnons, which are always present even in the ground state of the AF, near the additionally created spin flip at time $t = 0$.

(ii) Unraveling why the spatiotemporal propagation of a magnon in the FM (AF) resembles the quantum walk (stone-in-pond) case, respectively. This is achieved by investigating the hopping amplitudes of a single magnon in real space. In the FM case, the situation is clear, since the Hamiltonian can be easily written in terms of bosons hopping on a lattice, $\hat{H} = \sum_{ij} T_{ij} \hat{a}_i^\dagger \hat{a}_j$ with hopping amplitudes $T_{ij} = 2J (\delta_{\mathbf{r}_i - \mathbf{r}_j} + \frac{1}{4} \delta_{\mathbf{r}_i - \mathbf{r}_j \pm \hat{x}} + \frac{1}{4} \delta_{\mathbf{r}_i - \mathbf{r}_j \pm \hat{y}})$, being

nonzero only for nearest-neighbor sites and within a given site (see Fig. 4a). This effective hopping matrix structure exactly defines a quantum walk problem. On the other hand, the AF Hamiltonian needs to be rewritten more carefully since the Bogolyubov transformation is required to eliminate magnon pair creation or annihilation terms. Consequently, the real-space representation is achieved by Fourier transforming the AF Hamiltonian written in the Bogolyubov magnons. We obtain $\hat{H} = \sum_{ij} T_{ij} \hat{\alpha}_i^\dagger \hat{\alpha}_j$, with $T_{ij} = \frac{1}{\sqrt{N}} \sum_{\mathbf{k}} \omega_{\mathbf{k}} e^{i\mathbf{k}(\mathbf{r}_i - \mathbf{r}_j)}$. From this it is clear that for the AF case, the tunneling amplitudes T_{ij} are nonzero to all sites on the same sub-lattice, though they decay with distance as $|\mathbf{r}_i - \mathbf{r}_j|$ (see Fig. 4b). Thus, one observes emergence of an isotropic circular shape of the spatiotemporal magnon density profile, just as in the case of a stone thrown into a pond.

Interestingly, the origin of such a particular long-range hopping amplitude in the AF lies in the interplay between the Bogolyubov transformation and the nearest-neighbor pair creation and annihilation present in the Hamiltonian written in the language of the original Holstein-Primakoff magnons, *i.e.*, before Bogolyubov transformation. The crucial observation here is that when a bosonic particle residing on site j is Bogolyubov-transformed to a bosonic hole, then the latter can reside on any site of the other sub-lattice than site j , but with a decaying probability with distance from site j . This is because we have the relation $\hat{a}_{\mathbf{r}_j}^\dagger \rightarrow \sum_l G(\mathbf{r}_{lj}) \hat{\alpha}_{\mathbf{r}_l}$, where $G(\mathbf{r}_{lj}) = \sum_{\mathbf{q}} \exp[i\mathbf{q}(\mathbf{r}_l - \mathbf{r}_j)] v_{-\mathbf{q}}$ and $v_{\mathbf{q}}$ is the relevant Bogolyubov coefficient. Thus, when the nearest-neighbor magnon pair creation is Bogolyubov-transformed to the creation of a hole and a particle, it yields nonzero transition coefficients T_{ij} connecting all sites on the same sub-lattice but with decaying values with increasing distance $|\mathbf{r}_i - \mathbf{r}_j|$, as discussed above.

(iii) Unfolding a relatively large, steady-in-time probability for detecting the excitation at the initial position in the AF case, as clearly visible by comparing the FM and the AF light cone distributions in Fig. 3. This specific dissimilarity is a direct consequence of the differences between the creation of magnons at the initial time in the FM and AF cases, already discussed above. In the FM state at time $t = 0$ there is just one point in space where the magnon is created and thus the magnon wave function spreads relatively fast from site \mathbf{r}_0 . In the AF case, on the other hand, the magnon is initially created at several sites, and hence the probability of finding the magnon at site \mathbf{r}_0 decreases relatively slowly with time.

In conclusion, we have presented an intriguingly simple way of characterizing prototypical magnetic ground states in quantum materials by their spacetime dynamics. We have shown that the ferromagnetic quantum walker is intimately tied to the quadratic magnon dispersion, whereas the antiferromagnetic walker has an emergent classical dynamics as for the stone thrown into a

pond, tied to its linear magnon dispersion like for classical acoustic sound or water waves. These deep connections, while not being too surprising after all, open important possibilities for studying the important quantum-magnetic properties of materials, besides the obvious potential realizations in quantum simulators. In particular, the subtle magnetic ground states in recently discovered two-dimensional van der Waals materials with CrI_3 [34] as a truly atomically thin ferromagnet, would make for interesting test objects of our predictions, provided that real-space and real-time imaging techniques can be pushed accordingly. Similarly, there are some well-known realizations of quasi two-dimensional Heisenberg antiferromagnets [35], and light-cone spreading has only recently been simulated in such systems [36]. A potential experimental probe is time-resolved resonant inelastic X-ray scattering, as proposed for instance in [37]. A further intriguing avenue for spacetime imaging is the opportunity to monitor Floquet-engineered magnetic exchange interactions [38, 39], which in turn would affect the light-cone-like dynamics [40]. We finally mention the intriguing possibility to investigate anomalous spin diffusion, similar to the anomalous charge diffusion reported in Ref. [41]), through spacetime dynamics.

Acknowledgments. Financial support by the DFG through the Emmy Noether program (SE 2558/2-1) is gratefully acknowledged. We kindly acknowledge support by the (Polish) National Science Center (NCN, Poland) under Projects No. 2016/22/E/ST3/00560 (PW and KW), 2016/23/B/ST3/00839 (KW), and 2016/22/E/ST2/00555 (TS).

* krzysztof.wohlfeld@fuw.edu.pl

† tomasz.sowinski@ifpan.edu.pl

‡ michael.sentef@mpsd.mpg.de

- [1] D. I. Khomskii, *Basic Aspects of the Quantum Theory of Solids: Order and Elementary Excitations* (Cambridge University Press, 2010).
- [2] I. Bloch, J. Dalibard, and W. Zwerger, *Rev. Mod. Phys.* **80**, 885 (2008).
- [3] M. Lewenstein, A. Sanpera, and V. Ahufinger, *Ultracold Atoms in Optical Lattices: Simulating quantum many-body systems* (Oxford University Press, Oxford, 2012).
- [4] U. Schneider, L. Hackermüller, S. Will, T. Best, I. Bloch, T. A. Costi, R. W. Helmes, D. Rasch, and A. Rosch, *Science* **322**, 1520 (2008).
- [5] R. Jördens, N. Strohmaier, K. Günter, H. Moritz, and T. Esslinger, *Nature* **455**, 204 (2008).
- [6] M. Greiner, O. Mandel, T. Esslinger, T. W. Hänsch, and I. Bloch, *Nature* **415**, 39 (2002).
- [7] J. Simon, W. S. Bakr, R. Ma, M. E. Tai, P. M. Preiss, and M. Greiner, *Nature* **472**, 307 (2011).
- [8] B. Yan, S. A. Moses, B. Gadway, J. P. Covey, K. R. A. Hazzard, A. M. Rey, D. S. Jin, and J. Ye, *Nature* **501**, 521 (2013).
- [9] W. S. Bakr, J. I. Gillen, A. Peng, S. Fölling, and M. Greiner, *Nature* **462**, 74 (2009).
- [10] J. F. Sherson, C. Weitenberg, M. Endres, M. Cheneau, I. Bloch, and S. Kuhr, *Nature* **467**, 68 (2010).
- [11] W. S. Bakr, A. Peng, M. E. Tai, R. Ma, J. Simon, J. I. Gillen, S. Fölling, L. Pollet, and M. Greiner, *Science* **329**, 547 (2010).
- [12] C. Weitenberg, M. Endres, J. F. Sherson, M. Cheneau, P. Schauß, T. Fukuhara, I. Bloch, and S. Kuhr, *Nature* **471**, 319 (2011).
- [13] E. Haller, J. Hudson, A. Kelly, D. A. Cotta, B. Peaudecerf, G. D. Bruce, and S. Kuhr, *Nature Physics* **11**, 738 (2015).
- [14] G. J. A. Edge, R. Anderson, D. Jervis, D. C. McKay, R. Day, S. Trotzky, and J. H. Thywissen, *Phys. Rev. A* **92**, 063406 (2015).
- [15] M. F. Parsons, A. Mazurenko, C. S. Chiu, G. Ji, D. Greif, and M. Greiner, *Science* **353**, 1253 (2016).
- [16] M. Boll, T. A. Hilker, G. Salomon, A. Omran, J. Nespolo, L. Pollet, I. Bloch, and C. Gross, *Science* **353**, 1257 (2016).
- [17] L. W. Cheuk, M. A. Nichols, K. R. Lawrence, M. Okan, H. Zhang, E. Khatami, N. Trivedi, T. Paiva, M. Rigol, and M. W. Zwierlein, *Science* **353**, 1260 (2016).
- [18] A. Mazurenko, C. S. Chiu, G. Ji, M. F. Parsons, M. Kanász-Nagy, R. Schmidt, F. Grusdt, E. Demler, D. Greif, and M. Greiner, *Nature* **545**, 462 (2017).
- [19] M. Karski, L. Förster, J.-M. Choi, A. Steffen, W. Alt, D. Meschede, and A. Widera, *Science* **325**, 174 (2009).
- [20] H. Schmitz, R. Matjeschk, C. Schneider, J. Glueckert, M. Enderlein, T. Huber, and T. Schaetz, *Phys. Rev. Lett.* **103**, 090504 (2009).
- [21] A. Peruzzo, M. Lobino, J. C. F. Matthews, N. Matsuda, A. Politi, K. Poulios, X.-Q. Zhou, Y. Lahini, N. Ismail, K. Wörhoff, Y. Bromberg, Y. Silberberg, M. G. Thompson, and J. L. O'Brien, *Science* **329**, 1500 (2010).
- [22] F. Zähringer, G. Kirchmair, R. Gerritsma, E. Solano, R. Blatt, and C. F. Roos, *Phys. Rev. Lett.* **104**, 100503 (2010).
- [23] S. E. Venegas-Andraca, *Quantum Information Processing* **11**, 1015 (2012).
- [24] Y. Lahini, M. Verbin, S. D. Huber, Y. Bromberg, R. Pugatch, and Y. Silberberg, *Phys. Rev. A* **86**, 011603 (2012).
- [25] P. M. Preiss, R. Ma, M. E. Tai, A. Lukin, M. Rispoli, P. Zupancic, Y. Lahini, R. Islam, and M. Greiner, *Science* **347**, 1229 (2015).
- [26] D. Wiater, T. Sowiński, and J. Zakrzewski, *Phys. Rev. A* **96**, 043629 (2017).
- [27] Y. Ye, Z.-Y. Ge, Y. Wu, S. Wang, M. Gong, Y.-R. Zhang, Q. Zhu, R. Yang, S. Li, F. Liang, J. Lin, Y. Xu, C. Guo, L. Sun, C. Cheng, N. Ma, Z. Y. Meng, H. Deng, H. Rong, C.-Y. Lu, C.-Z. Peng, H. Fan, X. Zhu, and J.-W. Pan, *Phys. Rev. Lett.* **123**, 050502 (2019).
- [28] Z. Yan, Y.-R. Zhang, M. Gong, Y. Wu, Y. Zheng, S. Li, C. Wang, F. Liang, J. Lin, Y. Xu, C. Guo, L. Sun, C.-Z. Peng, K. Xia, H. Deng, H. Rong, J. Q. You, F. Nori, H. Fan, X. Zhu, and J.-W. Pan, *Science* **364**, 753 (2019).
- [29] S. Mondal and T. Mishra, "Spontaneous quantum walk reversal of bosonic mott insulator defects," (2020), arXiv:2001.08527 [cond-mat.quant-gas].
- [30] A. Auerbach, *Interacting Electrons and Quantum Magnetism* (Springer, New York, 1994).
- [31] M. Mourigal, M. E. Zhitomirsky, and A. L. Chernyshev, *Phys. Rev. B* **82**, 144402 (2010).

- [32] Supplementary material available.
- [33] E. H. Lieb and D. W. Robinson, *Commun.Math. Phys.* **28**, 251 (1972).
- [34] B. Huang, G. Clark, E. Navarro-Moratalla, D. R. Klein, R. Cheng, K. L. Seyler, D. Zhong, E. Schmidgall, M. A. McGuire, D. H. Cobden, W. Yao, D. Xiao, P. Jarillo-Herrero, and X. Xu, *Nature* **546**, 270 (2017).
- [35] B. Dalla Piazza, M. Mourigal, N. B. Christensen, G. J. Nilsen, P. Tregenna-Piggott, T. G. Perring, M. Enderle, D. F. McMorrow, D. A. Ivanov, and H. M. Rønnow, *Nature Physics* **11**, 62 (2015).
- [36] G. Fabiani and J. H. Mentink, arXiv:1912.10845 (2019).
- [37] Y. Wang, C. J. Jia, B. Moritz, and T. P. Devereaux, *Phys. Rev. Lett.* **112**, 156402 (2014).
- [38] J. H. Mentink, K. Balzer, and M. Eckstein, *Nature Communications* **6**, 6708 (2015).
- [39] D. M. Kennes, A. de la Torre, A. Ron, D. Hsieh, and A. J. Millis, *Physical Review Letters* **120**, 127601 (2018).
- [40] M. H. Kalthoff, D. M. Kennes, and M. A. Sentef, *Phys. Rev. B* **100**, 165125 (2019).
- [41] M. Mitrano, A. A. Husain, S. Vig, A. Kogar, M. S. Rak, S. I. Rubeck, J. Schmalian, B. Uchoa, J. Schneeloch, R. Zhong, G. D. Gu, and P. Abbamonte, *PNAS* **115**, 5392 (2018).

Quantum walk versus stone in pond: Distinguishing ground states of quantum magnets by spacetime dynamics

SUPPLEMENTARY MATERIAL

Piotr Wrzosek¹, Krzysztof Wohlfeld¹, Tomasz Sowiński², and Michael A. Sentef³

¹ *Faculty of Physics, University of Warsaw, Pasteura 5, PL-02093 Warsaw, Poland*

² *Institute of Physics, Polish Academy of Sciences, Aleja Lotników 32/46, PL-02668 Warsaw, Poland*

³ *Max Planck Institute for the Structure and Dynamics of Matter, Luruper Chaussee 149, D-22761 Hamburg, Germany*

MODEL AND LINEAR SPIN-WAVE THEORY

The spin Hamiltonian, which describes both 2D ferro- and antiferromagnets, reads

$$\hat{H} = J \sum_{\langle i,j \rangle} \hat{\mathbf{S}}_i \cdot \hat{\mathbf{S}}_j + h \sum_i \hat{S}_i^z, \quad (4)$$

with nearest-neighbor spin exchange interaction $J > 0$ on a 2D square lattice for spins $S = \frac{1}{2}$. This Hamiltonian is equivalent to the 2D antiferromagnetic Heisenberg model when the external magnetic field vanishes $h = 0$, while for $h \geq h_c = 4J$ it describes the ferromagnetic model [30, 31]. Introducing magnons via the standard Holstein-Primakoff transformation and performing linear spin-wave theory

$$\hat{S}_j^z = \frac{1}{2} - \hat{a}_j^\dagger \hat{a}_j, \quad (5a)$$

$$\hat{S}_j^+ \approx \hat{a}_j, \quad (5b)$$

$$\hat{S}_j^- \approx \hat{a}_j^\dagger, \quad (5c)$$

we obtain a noninteracting bosonic model which reads

$$\begin{aligned} \hat{H} = & h \sin \theta \sum_i \hat{a}_i^\dagger \hat{a}_i + \frac{J}{2} \sum_{\langle i,j \rangle} \left[\cos 2\theta (\hat{a}_i^\dagger \hat{a}_i + \hat{a}_j^\dagger \hat{a}_j) \right. \\ & \left. + \sin^2 \theta (\hat{a}_i^\dagger \hat{a}_j + \hat{a}_j^\dagger \hat{a}_i) - \cos^2 \theta (\hat{a}_i^\dagger \hat{a}_j^\dagger + \hat{a}_j \hat{a}_i) \right], \quad (6) \end{aligned}$$

where $\sin \theta = h/4J$. The ground state of the system is purely antiferromagnetic for $\theta = 0$. For $0 < \theta < \frac{\pi}{2}$ the ground state is a canted antiferromagnet, which is not investigated here. Once $\theta = \frac{\pi}{2}$ ($h = h_c$) the ground state is fully ferromagnetically polarized. The diagonal form of \hat{H} is obtained through Fourier and Bogolyubov transformations, with the latter defined as

$$\hat{a}_{\mathbf{k}} = u_{\mathbf{k}} \hat{\alpha}_{\mathbf{k}} + v_{\mathbf{k}} \hat{\alpha}_{-\mathbf{k}}^\dagger. \quad (7)$$

This way we obtain a diagonal form in terms of the Bogolyubov magnons,

$$\hat{H} = \sum_{\mathbf{k}} \omega_{\mathbf{k}} \hat{\alpha}_{\mathbf{k}}^\dagger \hat{\alpha}_{\mathbf{k}} + \frac{1}{2} \sum_{\mathbf{k}} (\omega_{\mathbf{k}} - A_{\mathbf{k}}), \quad (8)$$

where

$$A_{\mathbf{k}} = 2J(1 + \gamma_{\mathbf{k}} \sin^2 \theta), \quad u_{\mathbf{k}}^2, v_{\mathbf{k}}^2 = \frac{A_{\mathbf{k}} \pm \omega_{\mathbf{k}}}{2\omega_{\mathbf{k}}}, \quad (9)$$

with the energy of the Bogolyubov magnons given as

$$\omega_{\mathbf{k}} = 2J\sqrt{(1 + \gamma_{\mathbf{k}})(1 - \gamma_{\mathbf{k}} \cos 2\theta)}, \quad (10)$$

and $\gamma_{\mathbf{k}} = \frac{1}{2}(\cos k_x + \cos k_y)$.

MAGNON DENSITY PROFILES: EQUATIONS

The main goal of the paper is to investigate how a single spin flip excitation on a given site \mathbf{r}_i on top of the ground state propagates in space and time. To this end, we calculate here the space-time dependence of a density profile $\rho(\mathbf{r}, t)$ of a single spin-flip excitation in a quantum magnet. As this is achieved in the magnon language, we first write down an equation for $\rho(\mathbf{r}, t)$ in terms of the Holstein-Primakoff magnons:

$$\rho(\mathbf{r}, t) = \langle \emptyset_\alpha | \hat{a}_{\mathbf{r}_0}(t) \hat{n}_{\mathbf{r}_i} \hat{a}_{\mathbf{r}_0}^\dagger(t) | \emptyset_\alpha \rangle, \quad (11a)$$

$$\hat{a}_{\mathbf{r}}^\dagger(t) = e^{-i\frac{\hat{H}}{\hbar}t} \hat{a}_{\mathbf{r}}^\dagger \sqrt{1 - \hat{a}_{\mathbf{r}}^\dagger \hat{a}_{\mathbf{r}}} e^{i\frac{\hat{H}}{\hbar}t}, \quad (11b)$$

where $\mathbf{r} = \mathbf{r}_i - \mathbf{r}_0$ and $|\emptyset_\alpha\rangle$ is the vacuum for Bogolyubov bosons α , *i.e.*, the ground state of the system. A spin flip that is performed on given site \mathbf{r}_i of the ground state is equivalent to the creation of a single magnon on that site provided that the site is not yet occupied by a magnon.

In the mean-field picture $\langle \hat{a}_{\mathbf{r}_0}^\dagger \hat{a}_{\mathbf{r}_0} \rangle = \Delta m$ and the density profile of a single magnon excitation reads

$$\rho(\mathbf{r}, t) \approx (1 - \Delta m) \langle \emptyset_\alpha | \hat{a}_{\mathbf{r}_0} e^{i\frac{\hat{H}}{\hbar}t} \hat{a}_{\mathbf{r}_i}^\dagger \hat{a}_{\mathbf{r}_i} e^{-i\frac{\hat{H}}{\hbar}t} \hat{a}_{\mathbf{r}_0}^\dagger | \emptyset_\alpha \rangle. \quad (12)$$

Performing Fourier and Bogolyubov transformations we arrive at the following equation for the magnon density

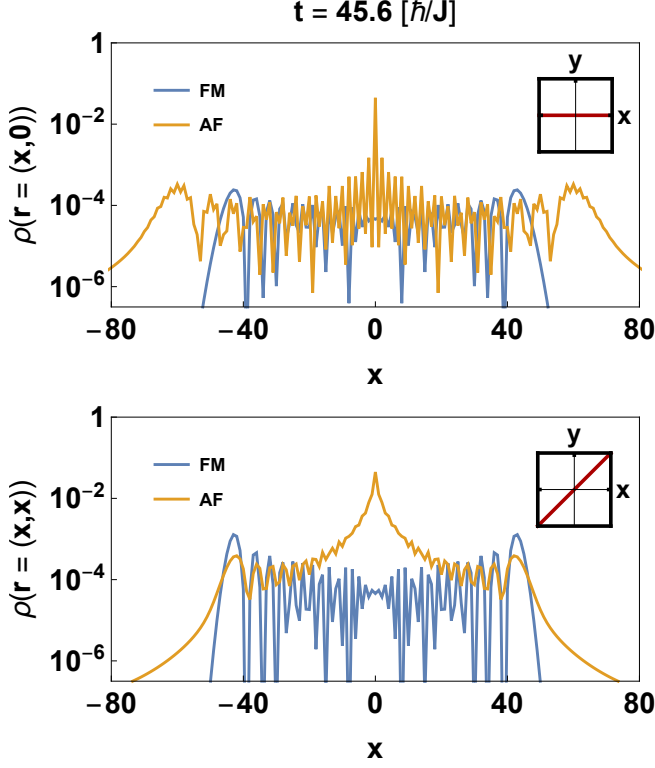


Figure S1. Magnon density profile $\rho(\mathbf{r}, t)$ at time $t = 45.6[\hbar/J]$. Top (bottom) panel shows cuts along the OX (diagonal) directions for the FM (blue) and AF (yellow) ground state, respectively.

profile,

$$\rho(\mathbf{r}, t) \approx \frac{1 - \Delta m}{N^2} \left(\left| \sum_{\mathbf{k}} u_{\mathbf{k}}^2 e^{i(\mathbf{k}\mathbf{r} - \omega_{\mathbf{k}}t)} \right|^2 + \left| \sum_{\mathbf{k}} u_{\mathbf{k}} v_{\mathbf{k}} e^{i(\mathbf{k}\mathbf{r} - \omega_{\mathbf{k}}t)} \right|^2 + \sum_{\mathbf{k}, \mathbf{q}} u_{\mathbf{k}}^2 v_{\mathbf{q}}^2 \right). \quad (13)$$

The last term, $\sum_{\mathbf{k}, \mathbf{q}} u_{\mathbf{k}}^2 v_{\mathbf{q}}^2$, is just a constant number describing the level of the quantum fluctuations present in the system. Since we are interested in the dynamics, in the figures we show only those parts of the density profile that are time-dependent,

$$\rho(\mathbf{r}, t) = \frac{1}{\mathcal{N}} \left| \sum_{\mathbf{k}} u_{\mathbf{k}}^2 e^{i(\mathbf{k}\mathbf{r} - \omega_{\mathbf{k}}t)} \right|^2 + \frac{1}{\mathcal{N}} \left| \sum_{\mathbf{k}} u_{\mathbf{k}} v_{\mathbf{k}} e^{i(\mathbf{k}\mathbf{r} - \omega_{\mathbf{k}}t)} \right|^2, \quad (14)$$

where \mathcal{N} is defined by $\sum_{\mathbf{r}} \rho(\mathbf{r}, t) = 1$.

MAGNON DENSITY PROFILES: ZOOM-IN AT FINITE TIME

Figure S1 shows a zoom-in into the magnon density profile $\rho(\mathbf{r}, t)$ at finite time. We observe that, as dis-

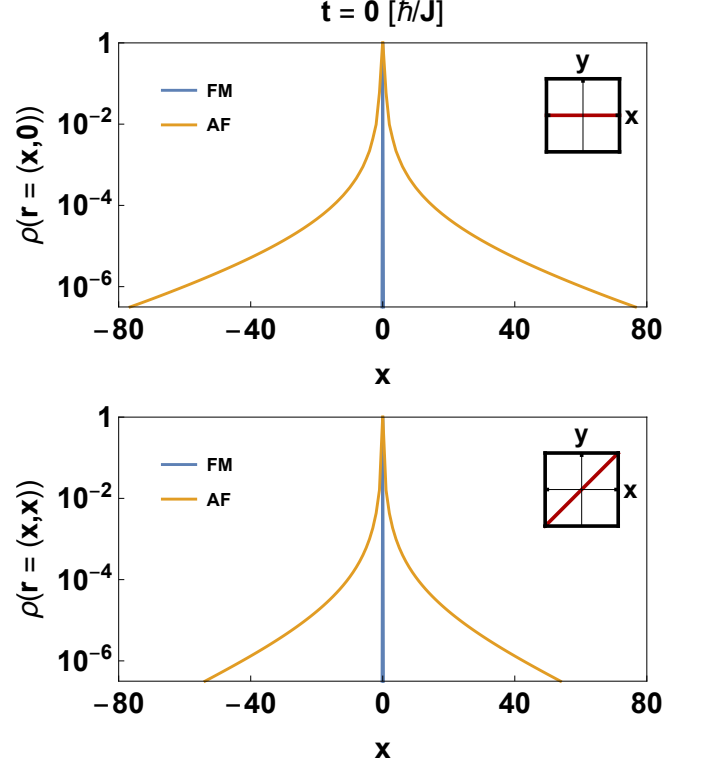


Figure S2. Magnon density profile $\rho(\mathbf{r}, t)$ at time $t = 0$. Top (bottom) panel shows cuts along the OX (diagonal) directions for the FM (blue) and AF (yellow) ground state, respectively.

cussed in the main text, there exists a non-zero probability to find a magnon outside of the light cone—not only in the AF (for which it could be quite easily expected) but also in the FM case. The latter is due to the fact that at a particular time t the higher order terms in the expansion of the magnon evolution operator $e^{-i\hat{H}t} \approx 1 + (-i\hat{H}t) + \frac{1}{2}(-i\hat{H}t)^2 + \dots$ are never completely suppressed.

MAGNON DENSITY PROFILES AT INITIAL TIME

The magnon density profile $\rho(\mathbf{r}, t)$ at time $t = 0$, i.e. at the time that a single spin flip is created, is shown in Fig. S2. As discussed in the main text, we observe that in the antiferromagnetic case a creation of a single spin flip at site \mathbf{r}_0 leads to a whole cloud of magnons being instantaneously created around this site. By contrast, this is not the case for a ferromagnet, for which the creation of a single spin flip at site \mathbf{r}_0 corresponds to just one single magnon instantaneously created at the same site and no magnons on other sites. We explain this phenomenon in two steps. (i) We express the creation operator of a single magnon at site \mathbf{r}_0 in terms of Bogolyubov magnons $\hat{\alpha}_{\mathbf{r}}$.

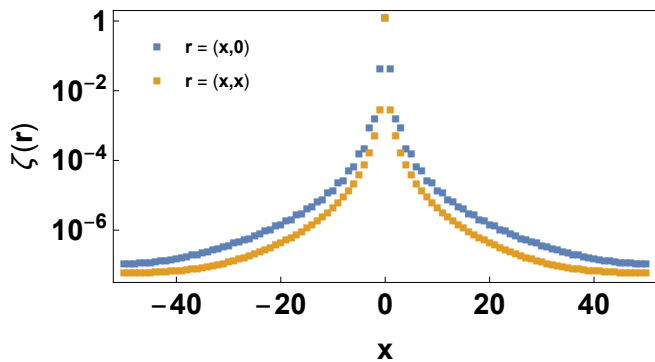


Figure S3. **Magnon density profile $\zeta(\mathbf{r})$ at time $t = 0$ of a single Bogolyubov boson in the AF ground state.** Blue and yellow dots show results along the OX and diagonal direction, respectively.

It then turns out that, creating a single magnon at site \mathbf{r}_0 is equivalent to the creation of a cloud of Bogolyubov magnons centered around \mathbf{r}_0 and with an exponentially decaying probability of finding them away from \mathbf{r}_0 . This is due to the combination of the Bogolyubov transformation and the relation

$$|a_{\mathbf{r}_j}\rangle = \sum_l \sum_{\mathbf{q}} u_{\mathbf{q}} \exp[i\mathbf{q}(\mathbf{r}_l - \mathbf{r}_j)] |a_{\mathbf{r}_l}\rangle \quad (15)$$

where $u_{\mathbf{q}}$ is the coefficient of the Bogolyubov transformation (9). (ii) It occurs that the density of magnons in a single Bogolyubov particle $|\alpha_{\mathbf{r}}\rangle$ also decays exponentially when going away from site \mathbf{r}_0 . Indeed the magnon density profile $\zeta(\mathbf{r})$ of a single Bogolyubov boson at time $t = 0$ defined as

$$\begin{aligned} \zeta(\mathbf{r}) &= \langle \emptyset_{\alpha} | \hat{a}_{\mathbf{r}_0} \hat{a}_{\mathbf{r}_i}^{\dagger} \hat{a}_{\mathbf{r}_i} \hat{a}_{\mathbf{r}_0}^{\dagger} | \emptyset_{\alpha} \rangle - \langle \emptyset_{\alpha} | \hat{a}_{\mathbf{r}_i}^{\dagger} \hat{a}_{\mathbf{r}_i} | \emptyset_{\alpha} \rangle \\ &= \left| \frac{1}{N} \sum_{\mathbf{k}} e^{i\mathbf{k}\mathbf{r}} u_{\mathbf{k}} \right|^2 + \left| \frac{1}{N} \sum_{\mathbf{k}} e^{i\mathbf{k}\mathbf{r}} v_{\mathbf{k}} \right|^2 \quad (16) \end{aligned}$$

is displayed in Fig. S3.

Altogether, the relation between the single spin flip created at site \mathbf{r}_0 of the AF ground state and the resulting distribution of magnons in such an excited state is a function of the product of the above two equations. This leads to the calculated magnon density profile (14) at time $t = 0$ and to the observed magnon density profile presented in Fig. S2. The intuitive understanding of this result is as follows: the AF Hamiltonian makes it energetically favorable to cluster the magnons (which are already present in the AF ground state) near the additionally created spin flip at time $t = 0$, as already stated in the main text of the paper.